Defect and Diffusion Forum
ISSN: 1662-9507, Vol. 451, pp 75-85
doi:10.4028/p-12AeQc

Submitted: 2026-01-12
Accepted: 2026-03-02
Online: 2026-04-17

Prediction of Temperature and Moisture Concentration in Autoclave-Cured Epoxy Resin Using Physics-Informed Neural Networks

Wancley O. Pedruzzi[1,a*], Igor F. Tosi[2,b], William P. M. Quiroz[4,c], Raffaele D'Elia[5,d], Julio C. S. Dutra[3,e], and Wellington B. da Silva[3,f]

[1]Graduate Program of Mechanical Engineering, Universidade Federal do Espírito Santo, Brazil.

[2]Graduate Program in Chemical Engineering, Universidade Federal do Espírito Santo, Brazil.

[3]Department of Rural Engineering, Universidade Federal do Espírito Santo, Brazil.

[4]Universidad San Sebastián, Campus Bellavista, Chile.

[5]Institut Clément Ader (ICA), Univ Toulouse, IMT Mines Albi, INSA Toulouse, ISAE Sup Aero, CNRS, ICA, Albi France.

[a]wancley.pedruzzi@edu.ufes.br, [b]igor.tosi@edu.ufes.br, [c]william.montes@uss.cl, [d]raffaele.delia@mines-albi.fr, [e]julio.dutra@ufes.br, [f]wellingtonufes@gmail.com

Keywords: PINNs, Composite, Porosity, Void Growth.

Abstract. Epoxy-based composites used in the aerospace industry are highly sensitive to moisture absorption, which can lead to porosity formation during the curing process and compromise structural integrity. Therefore, accurate prediction of temperature fields, degree of cure, and moisture concentration is essential for process optimization and defect mitigation. However, classical numerical approaches for solving the coupled governing equations are computationally expensive, limiting their applicability in real-time analyses and optimization strategies. In this work, Physics-Informed Neural Networks (PINNs) are investigated for predicting the transient thermal behavior, cure kinetics, and moisture concentration in an epoxy composite laminate during autoclave curing. Two PINNs are developed: the first solves the coupled transient heat transfer and cure kinetics equations in a composite-tooling system, while the second predicts the moisture concentration field in the laminate using the temperature information provided by the first network. Different network architectures are evaluated, and their performance is compared with numerical solutions obtained via the Finite Volume and Finite Element Methods. The results demonstrate that PINNs accurately reproduce temperature profiles, degree of cure, and moisture concentration, achieving high coefficients of determination, while also providing significant computational efficiency advantages during the prediction stage. These findings highlight the potential of PINNs as a robust and efficient tool for modeling complex coupled phenomena in composite manufacturing processes.

Introduction

Epoxy-based composites are widely employed in the aerospace industry in processes such as autoclave lamination, due to their ability to produce high-performance components with superior structural quality. However, these materials are sensitive to moisture absorption, which promotes porosity formation during curing and may compromise their properties, ultimately leading to part rejection [1].

Mitigating this issue requires strict control of process parameters, particularly pressure and temperature. In this context, modeling and computational simulation stand out as essential tools for parameter estimation and optimization. The prediction of void growth involves the coupling of differential equations [1, 2], whose solution is computationally expensive and limits their application in control and optimization strategies. Within this scenario, data-driven approaches emerge as an alternative to classical modeling.

Among these, Physics Informed Neural Networks (PINNs) are an emerging and promising alternative to solve differential equations, as introduced by [3], [4] and [5].

PINNs share a structure similar to that of traditional artificial neural networks, comprising input and output layers, hidden layers, and activation functions. The main distinction lies in the incorporation of physical laws into the modeling process. This is achieved by adding a term to the loss function that penalizes deviations from these physical laws, such as governing differential equations, thereby ensuring that the network predictions remain consistent with known physical principles. Other important aspects of PINNs include weight initialization [6], loss functions [7], network depth and number of neurons [8], and overfitting [9].

In this sense, the present work investigates the application of PINNs for predicting temperature and concentration fields. Two neural networks are employed, the first is designed to solve the transient heat equation coupled with the resin degree of cure, while the second PINN is constructed to compute the moisture concentration using Fick's second law, aiming to provide a solid foundation for rapid system state predictions and for estimating viscosity and void growth through external models.

Physical Problem and Mathematical Formulation

The model developed in this work is based on those presented by [2] and [1]. It consists of an energy balance for temperature calculation, accounting for heat transfer through the composite laminate and the tooling, as well as the exothermic effect of the resin chemical reaction during curing. A mass balance is also included to determine the moisture concentration distribution along the composite thickness during the autoclave curing cycle, together with a kinetic model used to predict the evolution of the degree of cure as a function of time and temperature. As illustrated in Figure 1, the model is applied to a one-dimensional domain comprising a laminate of thickness L and a metallic tool of thickness s. The kinetic model adopted to describe resin curing corresponds to a modified version

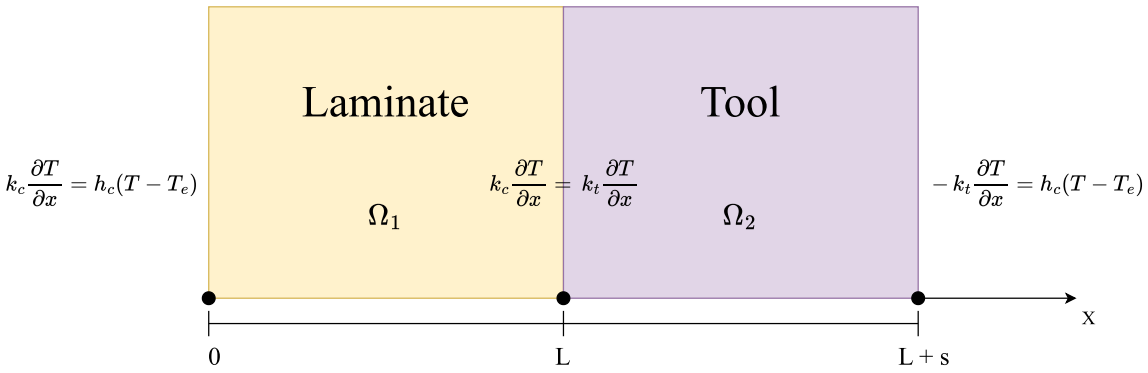

Fig. 1: Schematic representation of the problem domain.

of the model originally proposed by [10], and later extensively examined by [11], [2], and [1]. This version accounts for the effects of resin vitrification during the curing process by introducing the term α_{max}, whose value ranges from 0 to 1.

$$\frac{d\alpha}{dt} = k_1(\alpha_{max} - \alpha)^{n_1} + k_2\alpha^m(\alpha_{max} - \alpha)^{n_2} \tag{1}$$

$$k_i = k_{0i}e^{-E_{ai}/RT} \tag{2}$$

$$\alpha_{max} = p + qT \tag{3}$$

where α (–) is the degree of cure of the resin, m (–), n_1 (–), and n_2 (–) are reaction orders, and k_1 (s^{-1}) and k_2 (s^{-1}) are kinetic constants with an Arrhenius-type dependence on temperature T (K). The parameters p (–) and q (K^{-1}) were fitted by [2].

To account for heat transfer through the composite laminate and the tooling, along with the exothermic effects of the resin chemical reaction during the curing process, an energy balance was introduced. For this model, a plane-parallel geometry with constant properties is assumed [2].

$$\rho_c c_{pc} \frac{\partial T}{\partial t} = k_c \frac{\partial^2 T}{\partial x^2} + \rho_c \Delta h_{ref} \frac{d\alpha}{dt}, \quad x \in \Omega_1 \tag{4}$$

$$\rho_t c_{pt} \frac{\partial T}{\partial t} = k_t \frac{\partial^2 T}{\partial x^2}, \quad x \in \Omega_2 \tag{5}$$

where ρ_c (kg/m³) is the density of the composite, c_{pc} (J/(kg·K)) its specific heat, k_c (W/(m·K)) its thermal conductivity, and Δh_{ref} (J/kg) the heat generated by the chemical reaction. Similarly, ρ_t (kg/m³) is the density of the tooling, c_{pt} (J/(kg·K)) its specific heat, and k_t (W/(m·K)) its thermal conductivity.

For the boundary conditions, lateral convection is considered at each end in contact with the autoclave internal gas, whose heating is modeled by a linear ramp with a slope of 2 °C/min, becoming asymptotic upon reaching 180 °C, the curing temperature. These boundary conditions are represented by Equations 6 and 7.

$$k_c \frac{\partial T}{\partial x} = h(T - Tout), \quad in \quad x = 0 \tag{6}$$

$$-k_t \frac{\partial T}{\partial x} = h(T - Tout), \quad in \quad x = L + s \tag{7}$$

For the concentration profile, Fick's second law was employed to calculate the moisture concentration C (mol/m³), defined as the absolute amount of absorbed moisture, expressed as the mass of moisture per unit volume.

$$\frac{\partial C}{\partial t} = D \frac{\partial^2 C}{\partial x^2}, \quad x \in \Omega_1 \tag{8}$$

where x (m) represents the direction along the thickness and D (m²/s) is the diffusivity, assumed independent of the spatial variable x. However, the moisture diffusivity is strongly influenced by temperature and, in the case of water diffusion in pre-cured or cured resin, follows an Arrhenius-type relationship.

$$D = D_0 e^{-E_{ad}/RT} \tag{9}$$

where D_0 (m²/s) is the pre-exponential constant, E_{ad} (J/mol) is the activation energy for diffusion per mole, R (J/(mol·K)) is the universal gas constant, and T (K) is the absolute temperature.

For the boundary conditions, a Dirichlet condition is applied at the left face and a Neumann condition at the right face, as described by Equation 10 and Equation 11, respectively.

$$C = 0, \quad in \quad x = 0 \tag{10}$$

$$\frac{\partial C}{\partial x} = 0, \quad in \quad x = L \tag{11}$$

The data corresponding to the parameters used in the deterministic approach of the model are presented in Table 1.

Table 1: Model parameters.

ρ_c ($\mathrm{kg\,m^{-3}}$)	c_{pc} ($\mathrm{J\,kg^{-1}\,K^{-1}}$)	k_c ($\mathrm{W\,m^{-1}\,K^{-1}}$)	ρ_t ($\mathrm{kg\,m^{-3}}$)	c_{pt} ($\mathrm{J\,kg^{-1}\,K^{-1}}$)	k_t ($\mathrm{W\,m^{-1}\,K^{-1}}$)
1.59×10^3	8.71×10^2	4.03×10^{-1}	2.70×10^3	9.00×10^2	1.45×10^2
Δh_{rf} ($\mathrm{J\,kg^{-1}}$)	h_c ($\mathrm{W\,m^{-2}\,K^{-1}}$)	k_{01} ($\mathrm{s^{-1}}$)	k_{02} ($\mathrm{s^{-1}}$)	E_{a1} ($\mathrm{J\,mol^{-1}}$)	E_{a2} ($\mathrm{J\,mol^{-1}}$)
3.56×10^5	40	1.15×10^{10}	1.40×10^2	1.27×10^5	4.51×10^4
R ($\mathrm{J\,mol^{-1}\,K^{-1}}$)	n_1 ($-$)	n_2 ($-$)	m ($-$)	p ($-$)	q ($\mathrm{K^{-1}}$)
8.314	7.90×10^{-1}	1.99	5.80×10^{-1}	-2.54	7.40×10^{-3}
D_0 ($\mathrm{m^2\,s^{-1}}$)	E_{ad} ($\mathrm{J\,mol^{-1}}$)	x_0 (m)	x_l (m)	x_s (m)	
1.90×10^{-2}	5.55×10^4	0	5.58×10^{-3}	$x_l + 2 \times 10^{-2}$	-

Physical-Informed Neural Network

Physics-Informed Neural Networks (PINNs) are machine learning techniques for solving differential equations [12]. In PINNs, the unknown solution is approximated by a neural network. The neural network is trained using data in a manner that satisfies the governing equation, as well as the initial and boundary conditions. This approach allows PINNs to directly incorporate physical laws and constraints into the neural network structure [3].

In this study, two Physics-Informed Neural Networks (PINNs) are developed with the aim of predicting the desired variables. In PINN 1, the input variables are x and t, and the outputs are temperature T and degree of cure α, considering two distinct regions. In region 1, both temperature and degree of cure are calculated, whereas in region 2, only the temperature is considered, as the degree of cure has no physical meaning. For PINN 2, the inputs are t, x, and T, with T being the temperature obtained as the output from PINN 1. The output of this network is the concentration field C. The architecture adopted is illustrated in Figure 2. The spatial domain is divided into two regions: Ω_1, corresponding

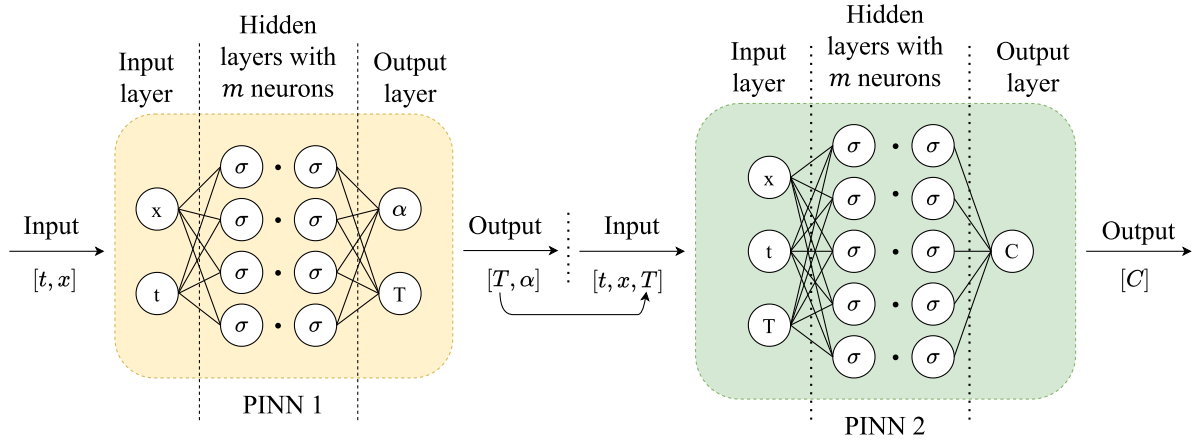

Fig. 2: Illustration of the inputs and output of the neural networks.

to the composite laminate, and Ω_2, corresponding to the Tool, separated by an interface located at $x = L$. The total loss function of PINN 1 is defined as the sum of the contributions associated with the governing equations in each region, the continuity conditions at the interface, and the boundary conditions, and is expressed as

$$\mathcal{L}_{\text{PINN1}} = \mathcal{L}_{\Omega_1} + \mathcal{L}_{\Omega_2} + \mathcal{L}_{\text{Interface}} + \mathcal{L}_{\text{BCs}} + \mathcal{L}_{\text{IC}} \tag{12}$$

In Region Ω_1, where the curing process takes place, heat transfer is coupled with the exothermic chemical reaction. Accordingly, the energy balance equation with the heat generation term and the kinetic equation for the degree of cure are imposed simultaneously. The residuals associated with these equations are defined as:

$$\mathcal{R}_T^{(1)}(t,x) = \rho_c c_{pc}\frac{\partial T}{\partial t} - k_c\frac{\partial^2 T}{\partial x^2} - \rho_c \Delta h_{ref}\frac{d\alpha}{dt}, \quad x \in \Omega_1 \tag{13}$$

$$\mathcal{R}_\alpha(t,x) = \frac{d\alpha}{dt} - \left[k_1(\alpha_{\max} - \alpha)^{n_1} + k_2\alpha^m(\alpha_{\max} - \alpha)^{n_2}\right], \quad x \in \Omega_1 \tag{14}$$

The contribution from Region 1 to the loss function is then given by

$$\mathcal{L}_{\Omega_1} = \left|\left|\mathcal{R}_T^{(1)}\right|\right|^2 + ||\mathcal{R}_\alpha||^2 \tag{15}$$

In Region Ω_2, corresponding to the tool, no chemical reaction occurs, and the physical process is governed exclusively by transient heat conduction. Thus, only the energy balance equation is imposed in this region, with the residual defined as

$$\mathcal{R}_T^{(2)}(t,x) = \rho_t c_{pt}\frac{\partial T}{\partial t} - k_t\frac{\partial^2 T}{\partial x^2}, \quad x \in \Omega_2 \tag{16}$$

The contribution from Region 2 to the loss function is expressed as

$$\mathcal{L}_{\Omega_2} = \left|\left|\mathcal{R}_T^{(2)}\right|\right|^2 \tag{17}$$

Although the neural network numerically provides values for the degree of cure α in Region 2 as well, no governing equation is imposed for this variable outside the composite. Therefore, the predicted values of α in Region 2 have no physical meaning and are not used in the energy balance, having no influence on the thermal solution.

At the interface between the two regions ($x = L$), physical continuity conditions are imposed to ensure the consistency of the thermal coupling between the composite and the tool. These conditions correspond to the continuity of temperature and heat flux, with the residuals defined as

$$\mathcal{R}_T^{\Gamma}(t) = T^{(1)}(L,t) - T^{(2)}(L,t) \tag{18}$$

$$\mathcal{R}_q^{\Gamma}(t) = k_c\left.\frac{\partial T}{\partial x}\right|_{L^-} - k_t\left.\frac{\partial T}{\partial x}\right|_{L^+} \tag{19}$$

The contribution associated with the interface is then given by

$$\mathcal{L}_{\text{Interface}} = \left|\left|\mathcal{R}_T^{\Gamma}\right|\right|^2 + \left|\left|\mathcal{R}_q^{\Gamma}\right|\right|^2 \tag{20}$$

The convective boundary conditions imposed on the external surfaces of the domain are incorporated into the loss function through the residuals

$$\mathcal{R}_{\text{BC}}^{0}(t) = k_c\frac{\partial T}{\partial x}(0,t) - h\left[T(0,t) - T_{out}(t)\right] \tag{21}$$

$$\mathcal{R}_{\text{BC}}^{L+s}(t) = -k_t\frac{\partial T}{\partial x}(L+s,t) - h\left[T(L+s,t) - T_{out}(t)\right] \tag{22}$$

The contribution of the boundary conditions to the total loss function is given by

$$\mathcal{L}_{BCs} = \left|\left|\mathcal{R}^{0}_{\text{BC}}\right|\right|^2 + \left|\left|\mathcal{R}^{L+s}_{\text{BC}}\right|\right|^2 \tag{23}$$

The initial conditions are incorporated into the loss function through the following residuals:

$$\mathcal{R}^{T}_{IC}(x) = T(x,0) - T_0, \quad x \in \Omega_1 \cup \Omega_2 \tag{24}$$

$$\mathcal{R}^{\alpha}_{IC}(x) = \alpha(x,0) - \alpha_0, \quad x \in \Omega_1 \tag{25}$$

The contribution of the initial conditions to the total loss function is then defined as

$$\mathcal{L}_{\text{IC}} = \left|\left|\mathcal{R}^{T}_{IC}\right|\right|^2 + ||\mathcal{R}^{\alpha}_{IC}||^2 \tag{26}$$

where the residuals are evaluated at the collocation points defined at the initial time $t = 0$.

For the concentration, this is defined only in Region Ω_1, corresponding to the composite laminate. Thus, the loss function of PINN 2 is formulated so as to enforce Fick's second law with diffusivity dependent on time, space, and temperature, as well as the boundary and initial conditions associated with the problem. The residual of the governing diffusion equation is defined as

$$\mathcal{R}_C(t,x) = \frac{\partial C}{\partial t} - D(T)\frac{\partial^2 C}{\partial x^2}, \quad x \in \Omega_1 \tag{27}$$

where $T = T(x,t)$ is the temperature predicted by PINN 1. The contribution associated with the governing equation to the loss function of PINN 2 is then expressed as

$$\mathcal{L}^{C}_{\Omega_1} = \|\mathcal{R}_C\|^2 \tag{28}$$

The boundary conditions of the diffusion problem are incorporated through additional residuals. On the left face of the domain ($x = 0$), a Dirichlet condition is imposed, defined as

$$\mathcal{R}^{0}_{BC,C}(t) = C(0,t), \tag{29}$$

while on the right face of the composite ($x = L$), a Neumann condition is imposed, expressed as

$$\mathcal{R}^{L}_{BC,C}(t) = \left.\frac{\partial C}{\partial x}\right|_{x=L} \tag{30}$$

The contribution of the boundary conditions to the loss function is then given by

$$\mathcal{L}^{C}_{BCs} = \left\|\mathcal{R}^{BC,0}_{C}\right\|^2 + \left\|\mathcal{R}^{BC,L}_{C}\right\|^2 \tag{31}$$

The initial conditions of the diffusion problem are likewise incorporated into the loss function. Considering a uniform initial concentration in the composite laminate, the residual associated with the initial condition is defined as

$$\mathcal{R}^{C}_{IC}(x) = C(x,0) - C_0, \quad x \in \Omega_1 \tag{32}$$

where C_0 represents the initial moisture concentration. The contribution of the initial conditions to the loss function of PINN 2 is then expressed as

$$\mathcal{L}^{C}_{IC} = \left\|\mathcal{R}^{C}_{IC}\right\|^2 \tag{33}$$

Thus, the total loss function associated with PINN 2 is defined as

$$\mathcal{L}_{\text{PINN2}} = \mathcal{L}^{C}_{\Omega_1} + \mathcal{L}^{C}_{BCs} + \mathcal{L}^{C}_{IC} \tag{34}$$

Table 2: Neural network architectures.

Number of hidden layers	Neurons per hidden layer
3, 5, 7	20, 40, 60, 80

For the computational implementation, the PINNs were developed using the TensorFlow framework, a library available in the Python programming language. Twelve distinct models were evaluated for each PINN, considering different combinations of layers and neurons in the hidden layers, as presented in Table 2.

In all cases, hyperbolic tangent (tanh) activation functions were employed in each layer, and the neural network weights were initialized using the Glorot uniform method, in which the weights of each layer are initialized from a uniform distribution as described by [13]. All terms of the loss function were weighted equally, with a weight of 1.0. The dataset used for training consisted of 15000 points for the partial differential equation domain residuals, 5500 points for the boundary conditions, and 1700 points for the initial conditions. These points were generated using a uniform sampling strategy.

The loss function was minimized through 60000 iterations of the Adam algorithm [14], with a learning rate of 10^{-3}, until convergence was achieved. After training, the prediction data were input into each model, and performance was evaluated using the Coefficient of Determination (R^2). For result verification, the Finite Volume Method (FVM) was employed in Python, as well as FlexPDE, a computational software with its own scripting language, developed for solving Partial Differential Equations (PDEs) using the Finite Element Method (FEM).

Results and Discussion

The PINN architectures were selected based on an architecture convergence assessment, in which the network performance varied according to the number of layers and the number of neurons per layer, as evaluated by the coefficient of determination (R^2) through comparison with the finite volume numerical solution. Table 3 reports this metric for architectures ranging from three to seven layers, with the number of neurons per layer varying from 20 to 80.

Table 3: Coefficient of determination (R^2) obtained for different PINN architectures.

Hidden layers	Neurons per layer	R^2 [-] (PINN 1)	R^2 [-] (PINN 2)
3	20	0.882	0.758
3	40	0.891	0.782
3	60	0.955	0.821
3	80	0.956	0.816
5	20	0.909	0.772
5	40	0.976	0.788
5	60	0.978	0.889
5	80	0.971	0.873
7	20	0.912	0.734
7	40	0.970	0.799
7	60	0.973	0.888
7	80	0.952	0.852

In Table 3, each proposed architecture is presented. It can be observed that increasing the number of neurons and layers leads to performance gains; however, there is a limit beyond which denser architectures no longer provide improvements. Specifically, for both PINN 1 and PINN 2, the best

performances were achieved with 5 layers and 60 to 80 neurons per layer. It is also noted that when 7 layers and 80 neurons were used, the networks exhibited reduced performance, which can be attributed to overfitting. In this context, the network with 5 layers and 60 neurons per layer was selected for PINN 1, and the network with 7 layers and 60 neurons per layer was selected for PINN 2. The loss function history is shown in Figure 3.

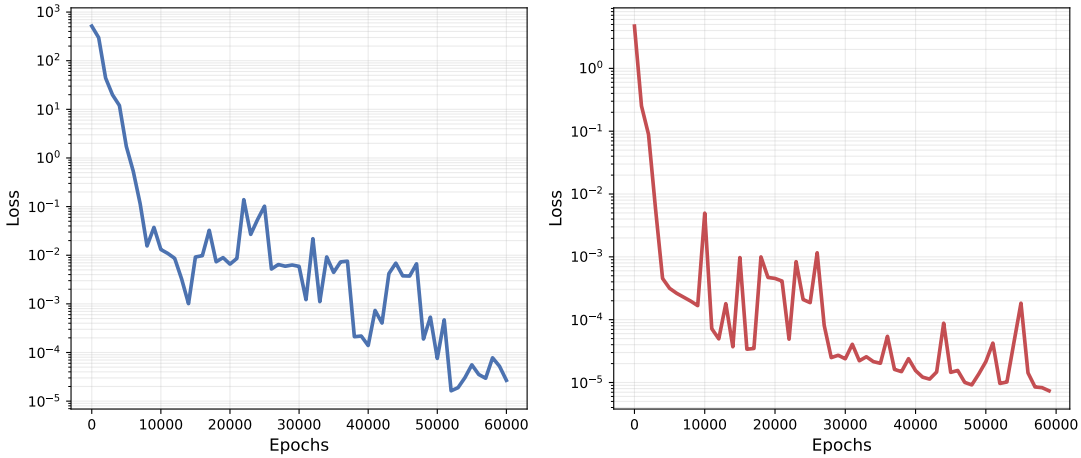

Fig. 3: Training history of the neural networks: PINN 1 (Left) and PINN 2 (Right).

It is important to note that, for all considered points, the loss function reaches the order of 10^{-4} to 10^{-5}, indicating that the physical model is respected within the observed domain.

Figure 4 illustrates the performance of the PINN 1 in predicting the temperature profile. It can be observed that the three solutions coincide, demonstrating the robustness of the tool, with an exceptional gain in computational cost. Classical methods, such as the finite volume method, discretize the problem and solve an $N \times N$ system of equations depending on the number of volumes, whereas the PINN incurs virtually no cost during prediction, despite being computationally intensive during training, a process performed offline.

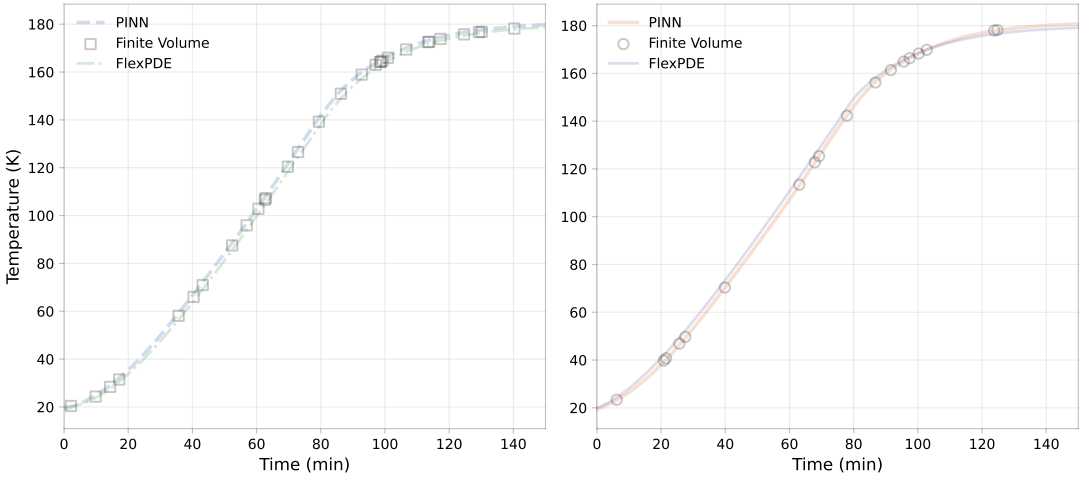

Fig. 4: Temperature profile: mid-plane (Left) and tool side (Right).

Regarding PINN 1, Figure 5 shows the prediction of the concentration field. In this case, it can be observed that the solutions coincide up to 75 minutes; after that, a slight divergence in the results occurs. This difference is reflected in the R^2 metric (Table 3) for the concentration profile. This network achieved slightly lower performance due to its complexity, its input couples the temperature, which

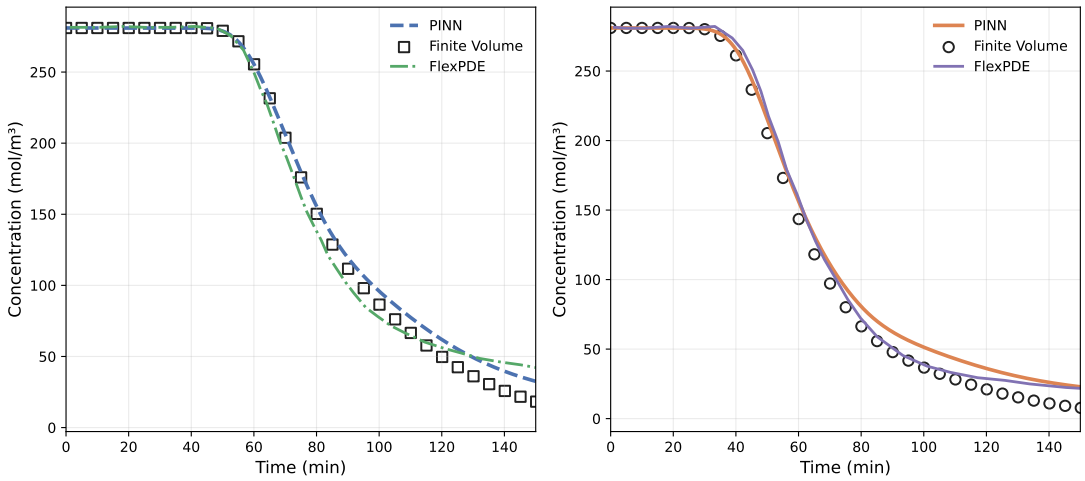

Fig. 5: Moisture concentration profile: mid-plane (left) and tool side (right).

is strongly linked to both space and time. Consequently, for each input temperature, a new profile emerges, increasing the complexity of the output.

With the PINNs properly trained, new opportunities for scientific investigation emerge, such as their application to the prediction of void growth in high-performance composites, using models such as those proposed by [15] and [16]. Another research direction involves the investigation of different hyperparameters, such as the activation function and the Latin hypercube sampling (LHS) strategy, in order to improve the quality of the solution obtained for the concentration field of PINN 2, as well as the proposal of a new architecture for PINN 1, which consists of its complete separation into two distinct networks, each responsible for a specific domain. Furthermore, an expansion of the input variables is proposed, in which the relevant parameters to be estimated are coupled, thereby characterizing the formulation of an inverse problem.

Conclusions

In this work, the application of Physics-Informed Neural Networks (PINNs) was evaluated for the coupled solution of heat transfer, cure kinetics, and moisture diffusion problems during the autoclave curing process of epoxy-based composite laminates. The proposed approach consisted of developing two distinct PINNs: the first aimed at predicting temperature and degree of cure fields in the composite–tooling system, and the second focused on determining the moisture concentration field in the laminate, using the thermal field provided by the first network as input.

The results indicate that PINN 1 is capable of accurately reproducing the temporal and spatial evolution of temperature and degree of cure, showing good agreement with reference numerical solutions obtained via the Finite Volume and Finite Element Methods. For PINN 2, it was observed that the prediction of the moisture concentration field is more sensitive to the network architecture due to the strong coupling between diffusivity and the space- and time-dependent temperature field, resulting in lower performance values compared to the thermal problem.

Analysis of different network architectures showed that increasing the number of layers and neurons per layer improves the approximation capability of the PINNs up to a certain limit, beyond which no further gains are observed and overfitting effects may occur. The selected architectures represent a compromise between accuracy and computational complexity.

Although the training process of the PINNs requires significant computational effort, this stage is performed offline. Once trained, the networks allow the fields of interest to be obtained without the need for iterative solution of the differential equations, which can be particularly relevant for applications requiring repeated system evaluations.

Finally, the presented methodology provides a consistent basis for future studies involving the extension of the model to predict void growth, the investigation of alternative training and sampling strategies, as well as the formulation of inverse problems for estimating parameters of the curing process in polymeric composites.

References

[1] Andrea Dei Sommi, Francesca Lionetto, Giuseppe Buccoliero, and Alfonso Maffezzoli. The effect of absorbed moisture and resin pressure on porosity in autoclave cured epoxy resin. *Polymer Composites*, 45(17):15793–15803, August 2024.

[2] Andrea Dei Sommi, Giuseppe Buccoliero, Francesca Lionetto, Fabio De Pascalis, Michele Nacucchi, and Alfonso Maffezzoli. A finite element model for the prediction of porosity in autoclave cured composites. *Composites Part B: Engineering*, 264:110882, September 2023.

[3] M. Raissi, P. Perdikaris, and G.E. E Karniadakis. Physics-informed neural networks: A deep learning framework for solving forward and inverse problems involving nonlinear partial differential equations. *Journal of Computational Physics*, 378:686–707, 2019.

[4] Maziar Raissi, Paris Perdikaris, and George Em Karniadakis. Physics Informed Deep Learning (Part I): Data-driven Solutions of Nonlinear Partial Differential Equations, 2017.

[5] Maziar Raissi, Paris Perdikaris, and George Em Karniadakis. Physics Informed Deep Learning (Part II): Data-driven Discovery of Nonlinear Partial Differential Equations, 2017.

[6] Jingjing Liu, Yefeng Liu, and Qichun Zhang. A weight initialization method based on neural network with asymmetric activation function. *Neurocomputing*, 483:171–182, April 2022.

[7] Yash Srivastava, Vaishnav Murali, and Shiv Ram Dubey. *A Performance Evaluation of Loss Functions for Deep Face Recognition*, page 322–332. Springer Singapore, 2020.

[8] S.H. Shabbeer Basha, Shiv Ram Dubey, Viswanath Pulabaigari, and Snehasis Mukherjee. Impact of fully connected layers on performance of convolutional neural networks for image classification. *Neurocomputing*, 378:112–119, February 2020.

[9] Qi Xu, Ming Zhang, Zonghua Gu, and Gang Pan. Overfitting remedy by sparsifying regularization on fully-connected layers of cnns. *Neurocomputing*, 328:69–74, February 2019.

[10] Musa R. Kamal. Thermoset characterization for moldability analysis. *Polymer Engineering amp; Science*, 14(3):231–239, March 1974.

[11] Panagiotis I. Karkanas and Ivana K. Partridge. Cure modeling and monitoring of epoxy/amine resin systems. i. cure kinetics modeling. *Journal of Applied Polymer Science*, 77(7):1419–1431, 2000.

[12] Zaharaddeen Karami Lawal, Hayati Yassin, Daphne Teck Ching Lai, and Azam Che Idris. Physics-informed neural network (pinn) evolution and beyond: A systematic literature review and bibliometric analysis. *Big Data and Cognitive Computing*, 6(4):140, 2022.

[13] Xavier Glorot and Yoshua Bengio. Understanding the difficulty of training deep feedforward neural networks. In Yee Whye Teh and Mike Titterington, editors, *Proceedings of the Thirteenth International Conference on Artificial Intelligence and Statistics*, volume 9 of *Proceedings of Machine Learning Research*, pages 249–256, Chia Laguna Resort, Sardinia, Italy, 13–15 May 2010. PMLR.

[14] Diederik P. Kingma and Jimmy Ba. Adam: A method for stochastic optimization, 2014.

[15] J. L. Kardos, M. P. Duduković, and R. Dave. *Void growth and resin transport during processing of thermosetting — Matrix composites*, page 101–123. Springer Berlin Heidelberg, 1986.

[16] Y. Ledru, G. Bernhart, R. Piquet, F. Schmidt, and L. Michel. Coupled visco-mechanical and diffusion void growth modelling during composite curing. *Composites Science and Technology*, 70(15):2139–2145, December 2010.